The following resources related to this article are available online at http://stke.sciencemag.org.
This information is current as of 8 February 2010.

Article Tools	Visit the online version of this article to access the personalization and article tools: **http://stke.sciencemag.org/cgi/content/full/sigtrans;2/102/ra84**
Supplemental Materials	*"Supplementary Materials"* **http://stke.sciencemag.org/cgi/content/full/sigtrans;2/102/ra84/DC1**
Related Content	The editors suggest related resources on *Science*'s sites: **http://stke.sciencemag.org/cgi/content/abstract/sigtrans;2/102/ra86** **http://stke.sciencemag.org/cgi/content/abstract/sigtrans;2/97/pe76**
References	This article cites 45 articles, 15 of which can be accessed for free: **http://stke.sciencemag.org/cgi/content/full/sigtrans;2/102/ra84#otherarticles**
Glossary	Look up definitions for abbreviations and terms found in this article: **http://stke.sciencemag.org/glossary/**
Permissions	Obtain information about reproducing this article: **http://www.sciencemag.org/about/permissions.dtl**

RESEARCH ARTICLE

CELL BIOLOGY

Regulation of Epidermal Growth Factor Receptor Trafficking by Lysine Deacetylase HDAC6

Yonathan Lissanu Deribe,[1] Philipp Wild,[1] Akhila Chandrashaker,[2]
Jasna Curak,[3] Mirko H. H. Schmidt,[1,4] Yannis Kalaidzidis,[2,5] Natasa Milutinovic,[3]
Irina Kratchmarova,[6] Lukas Buerkle,[3,7] Michael J. Fetchko,[3] Philipp Schmidt,[1]
Saranya Kittanakom,[3] Kevin R. Brown,[8] Igor Jurisica,[8,9,10] Blagoy Blagoev,[6]
Marino Zerial,[2] Igor Stagljar,[3]* Ivan Dikic[1,11,12]*

Binding of epidermal growth factor (EGF) to its receptor leads to receptor dimerization, assembly of protein complexes, and activation of signaling networks that control key cellular responses. Despite their fundamental role in cell biology, little is known about protein complexes associated with the EGF receptor (EGFR) before growth factor stimulation. We used a modified membrane yeast two-hybrid system together with bioinformatics to identify 87 candidate proteins interacting with the ligand-unoccupied EGFR. Among them was histone deacetylase 6 (HDAC6), a cytoplasmic lysine deacetylase, which we found negatively regulated EGFR endocytosis and degradation by controlling the acetylation status of α-tubulin and, subsequently, receptor trafficking along microtubules. A negative feedback loop consisting of EGFR-mediated phosphorylation of HDAC6 Tyr^{570} resulted in reduced deacetylase activity and increased acetylation of α-tubulin. This study illustrates the complexity of the EGFR-associated interactome and identifies protein acetylation as a previously unknown regulator of receptor endocytosis and degradation.

INTRODUCTION

The epidermal growth factor receptor (EGFR) is implicated in the regulation of crucial cellular functions ranging from cell growth, proliferation, and differentiation to cell survival (*1–3*). Critical steps that ensure propagation of extracellular signals within the cell include ligand-induced dimerization followed by tyrosine transphorylation (*4*). Intracellular signal transduction involves a large network of receptor-associated proteins, as previously shown by proteomic analyses that identified more than 100 proteins associated with ligand-activated receptors (*5, 6*). Activated ligand-receptor complexes are internalized and trafficked through a series of endocytic compartments where they are sorted for proteolytic degradation in the lysosome (*7–9*).

EGFR associates with specific proteins before growth factor stimulation, such as ZPR1, a zinc finger protein bound to the cytoplasmic tyrosine kinase domain of the EGFR, which is released from the receptor after activation, leading to the accumulation of ZPR1 in the cell nucleus (*10*). To explore the ligand-unoccupied EGFR protein interactome, we applied MYTH, the split ubiquitin (Ub)–based membrane yeast two-hybrid assay. MYTH allows the systematic analysis of full-length membrane protein interactions in a cellular environment. MYTH was useful in analyzing large membrane-anchored proteins, such as ion channels, G protein (heterotrimeric guanosine triphosphate–binding protein)–coupled receptors, and membrane transporters from yeast and plants (*11–13*). However, success with single-pass mammalian transmembrane proteins has been limited, largely because of improper incorporation of type I mammalian membrane proteins in yeast.

Here, we modified the MYTH system to make it amenable for screening of single-pass transmembrane proteins. We then used it to search for previously unknown EGFR-interacting proteins. We identified 87 proteins that bound to the receptor in a ligand-independent fashion and validated the complete set with bioinformatics and a subset by immunoprecipitation. Among these EGFR-interacting proteins was the cytoplasmic lysine deacetylase HDAC6 (histone deacetylase 6). We showed that HDAC6 modulated EGFR trafficking primarily by regulating the acetylation status of microtubules. We also identified a feedback mechanism where EGFR inactivated HDAC6 by phosphorylating it on Tyr^{570}. These findings implicate posttranslational modification by acetylation as a regulatory mechanism in EGFR trafficking and extend the use of membrane yeast two-hybrid screening as an investigational tool to study receptor tyrosine kinases.

[1]Institute of Biochemistry II and Cluster of Excellence Macromolecular Complexes, Goethe University School of Medicine, Theodor-Stern-Kai 7, D-60590 Frankfurt (Main), Germany. [2]Max-Planck-Institute of Molecular Cell biology and Genetics, Pfotenhauerstrasse 108, 01307 Dresden, Germany. [3]Departments of Biochemistry and Molecular Genetics, Terrence Donnelly Centre for Cellular and Biomolecular Research (CCBR), University of Toronto, 160 College Street, Room 1204, Toronto, Ontario, Canada M5S 3E1. [4]Laboratory for Tumor Biochemistry, Institute of Neurology (Edinger Institute), Goethe University School of Medicine, Heinrich-Hoffmann-Strasse 7, D-60528 Frankfurt (Main), Germany. [5]N. Belozersky Institute of Physico-Chemical Biology, Building A, Moscow State University, Moscow 119899, Russia. [6]Center for Experimental Bioinformatics, Department of Biochemistry and Molecular Biology, University of Southern Denmark, Campusvej 55, DK-5230 Odense, Denmark. [7]Institute of Plant Science, ETH Zurich, CH-8092 Zurich, Switzerland. [8]Division of Signaling Biology, Ontario Cancer Institute, Princess Margaret Hospital–University Health Network, 101 College Street, Toronto Medical Discovery Tower, 9-305, Toronto, Ontario, Canada M5G 1L7. [9]Department of Computer Science, University of Toronto, Toronto, Ontario, Canada M5S 1A4. [10]Department of Medical Biophysics, University of Toronto, Toronto, Ontario, Canada M5G 2M9. [11]Tumor Biology Program, Mediterranean Institute for Life Sciences, Mestrovicevo setaliste bb, 21000 Split, Croatia. [12]Department of Immunology, School of Medicine, University of Split, Soltanska 2, 21000 Split, Croatia.
*To whom correspondence should be addressed. E-mail: Ivan.Dikic@biochem2.de (I.D.) and igor.stagljar@utoronto.ca (I.S.)

RESULTS

A modified MYTH system reveals previously unknown interaction partners of EGFR

Expression of human EGFR fused to the C-terminal part of Ub (Cub) and a transcription factor (TF) (EGFR-C-T) in yeast caused a strong self-activation phenotype and the protein was substantially degraded in vivo (fig. S1, A and B). To circumvent this problem, we developed a modified version of the MYTH system that is more suitable for mammalian single-pass transmembrane receptors. Addition of the signal sequence of yeast α-mating pheromone precursor (MFα) to the EGFR protein devoid of its endogenous cleavable signal sequence (MFα-EGFR-C-T) led to stable expression of the MFα-EGFR-C-T chimeric protein (fig. S1B, lane 3), which was inserted into the plasma membrane, on the basis of ultracentrifugation (fig. S2E). We confirmed MFα-EGFR-C-T expression, and lack of self-activation, in yeast with the NubG/I test. The wild-type Nub isoform (NubI) has high affinity for Cub and, thus, these two moieties spontaneously reassociate in vivo in a manner that is independent of proteins fused to them. This NubI-Cub reassociation activates the MYTH reporter system (*ADE2/HIS3*/β-galactosidase). Growth on selective media confirms bait protein expression (fig. S1D). Introduction of the point mutation Nub I13G prevents the spontaneous NubG-Cub association. The split Ub moieties reconstitute only when proteins that are fused to the Cub and NubG interact, unless the bait protein is self-activating (that is, activating the MYTH reporter system in the absence of a bone fide protein interaction). The absence of growth with MFα-EGFR-C-T and NubG chimeras demonstrates that EGFR is not self-activating in yeast, which shows that it is amenable to study with MYTH (fig. S1D). Immunofluorescence analysis showed that MFα-EGFR-C-T was localized predominantly in the plasma membrane of yeast cells (fig. S1C). We did not detect tyrosine phosphorylation of EGFR in yeast lysates expressing the MFα-EGFR-C-T bait in Western blots with an antibody that recognizes tyrosine-phosphorylated EGFR (fig. S1F).

To identify EGFR-interacting partners, the MFα-EGFR-C-T construct was used as a bait protein in large-scale MYTH screens. From three independent screens totaling ~3 × 10^7 yeast transformants, 295 colonies were positive for the activation of the *HIS3^+/ADE2^+/lacZ^+* reporter genes. The specificity of these interactions was then evaluated through the bait-dependency test. Using the unrelated human plasma membrane protein transferrin receptor (TFRC) as a negative control, we ensured that the prey proteins interacted specifically with EGFR as a result of their affinity for the original bait (MFα-EGFR-C-T). The bait-dependency screen refined the number of EGFR-interacting proteins to 87, which we call the "EGFR-MYTH interactome" and which were further evaluated with a combination of bioinformatics, biochemical, and functional tests. The proteins comprising the EGFR-MYTH-interactome (table S1) fall into multiple Gene Ontology (GO) biological function groups, including those that play a role in cell fate and organization (green nodes), metabolism (yellow and gray nodes), protein degradation (protein fate, light blue nodes) and proteins with yet undefined functions (white nodes) (Fig. 1A). Fourteen of the EGFR-interacting partners are annotated as either integral membrane or membrane-associated proteins, showing the utility of the modified MYTH system for the identification of membrane proteins as EGFR-binding partners.

To further annotate and support the observed protein interactions, we compared our data with data from other experimental studies. We identified significant domain-domain co-occurrences, gene coexpressions, and computed functional similarity of interacting protein pairs (see Materials and Methods for details). MYTH identified 87 interactions with ligand-unoccupied EGFR, of which 11 proteins were com-mon to the 327 proteins previously identified as interacting with EGFR activated by growth factor stimulation (Fig. 1B and fig. S2). Support for 34 EGFR interactions identified in the MYTH screen came from analysis of a set of InterPro interaction domain pairs, which showed significant co-occurrence in known human protein interactions (see Materials and Methods for details). With GO (biological process, molecular function, cellular localization), we computed semantic similarity for all protein-protein interaction pairs (see Materials and Methods for details), which provided further computational validation for 62 of the MYTH-identified interactions (table S1). Finally, 32 of the MYTH-identified interactions link previously reported EGFR-interacting proteins (Fig. 1A, red edges), many of which have multiple lines of evidence (thick edges), thus further supporting their biological relevance to EGFR.
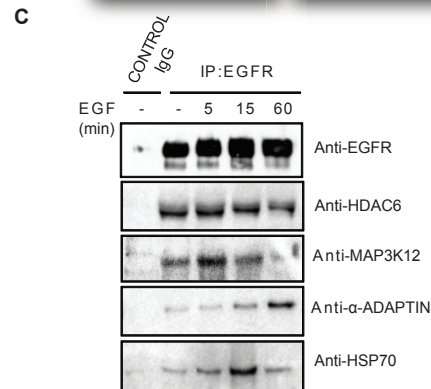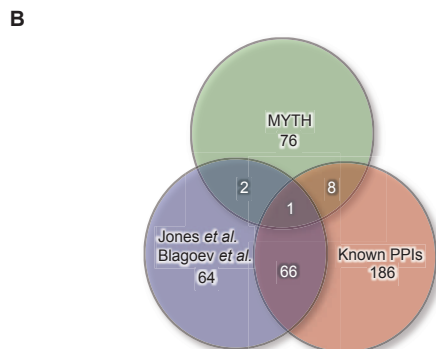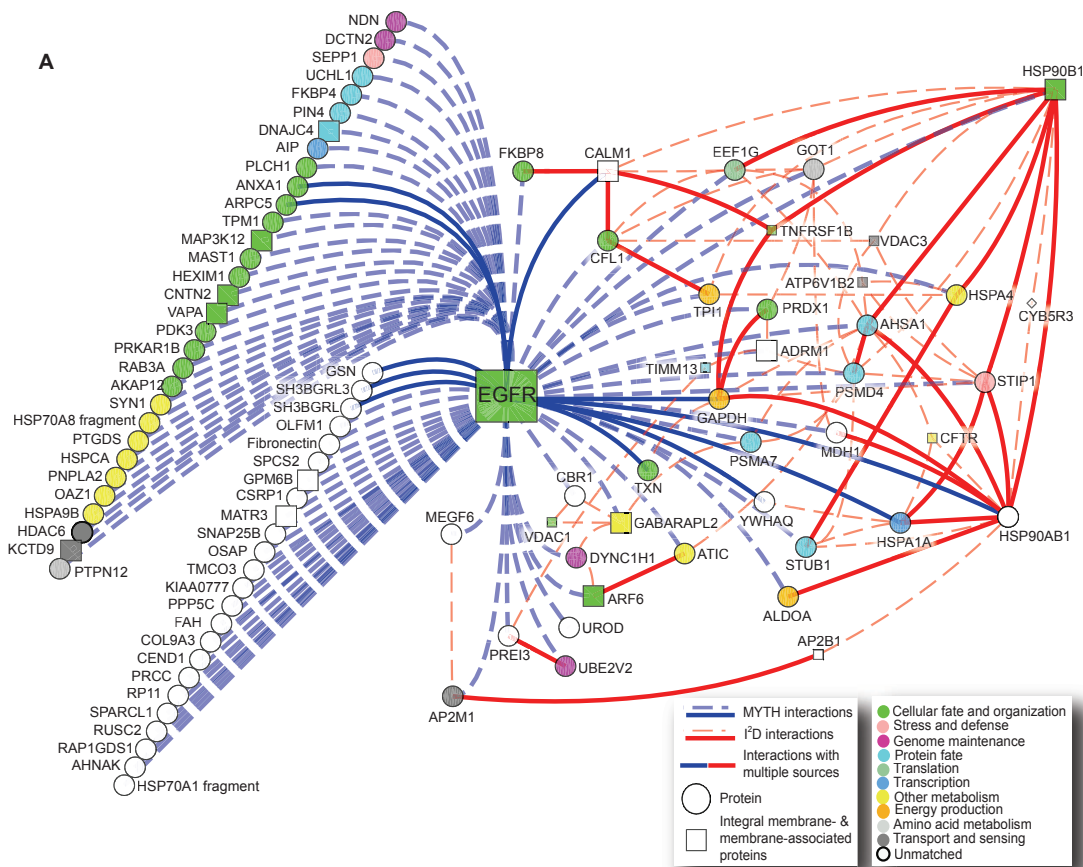
Several candidate interactors identified in the yeast screen were validated for their ability to bind to EGFR in mammalian cells. HDAC6, α-adaptin, heat shock protein 70 kD (HSP70), and mitogen-activated protein kinase kinase kinase 12 (MAP3K12) were coprecipitated with endogenous EGFR in nonstimulated A431 cells (Fig. 1C). The abundance of HDAC6 associated with the receptor before and after ligand stimulation was similar. Conversely, the interaction with α-adaptin was enhanced upon receptor stimulation, whereas that of MAP3K12 and HSP70 transiently increased and subsequently declined to the basal level. We confirmed that a member of the immunophilin family, FKBP38, and the adaptor 14-3-3θ formed complexes with EGFR when overexpressed in human embryonic kidney (HEK) 293T cells (fig. S3A) and that the Ub-like modifier GATE-16 interacted with EGFR by pull-down assay (fig. S3B). Additional putative EGFR-interacting proteins identified by MYTH screen were fused to enhanced green fluorescent protein (EGFP) and tested for their interactions with endogenous EGFR in HeLa cells. We detected interactions of 10 fusion proteins with the EGFR in nonstimulated cells (fig. S3C). Together, two distinct approaches based on entirely different principles (biochemical interaction–coimmunoprecipitation or pull-down assay and bioinformatics) validated the EGFR interactors identified with the modified MYTH system.

The cytoplasmic lysine deacetylase HDAC6 interacts with EGFR

We next focused our studies on HDAC6 that binds to EGFR to a similar extent under basal and stimulated conditions. HDAC6 contains two tandem deacetylase domains and a Ub-binding zinc finger domain (ZnF-UBP) and is predominantly localized in the cytoplasm (14). HDAC6 deacetylates and regulates α-tubulin, HSP90, and cortactin and modulates human immunodeficiency virus 1 (HIV-1) infection (15–18). The specificity of the EGFR/HDAC6 interaction was tested with the MYTH assay. Coexpression of the MFα-EGFR-C-T bait and the NubG-HDAC6 prey yielded robust growth under selection conditions and high activity in a β-galactosidase assay (Fig. 2A). This interaction was specific because no interaction of the MFα-EGFR-C-T bait was observed with an unrelated prey GABAβ1A (γ-aminobutyric acid β1A) fused to NubG, and, conversely, NubG-HDAC6 did not interact with the unrelated human transferrin receptor (T-C-TFRC) bait (Fig. 2A). Coimmunoprecipitation studies in mammalian cells confirmed a specific interaction of EGFR (fig. S4A) or of a kinase-deficient mutant of EGFR K721 with FLAG-HDAC6 upon overexpression (fig. S4B), further supporting the ability of HDAC6 to interact with EGFR irrespective of activation status. Endogenous HDAC6 and EGFR also interacted (Fig. 1C and fig. S4C).

To map the binding site for EGFR on HDAC6, we generated six HDAC6 deletions tagged with NubG and assessed their ability to interact with EGFR in the MYTH assay (Fig. 2B). As scored by growth on selective media and β-galactosidase activity (blue coloration), the interaction was maintained in the short construct containing HDAC6 amino acids 1010 to 1050, which

Fig. 1. Application of a modified MYTH system to the human EGFR. (**A**) An EGFR-interactome was identified with a modified MYTH system. All proteins from the MYTH screen were mapped into SwissProt identifiers and integrated with interactions in I²D version 1.71 (see Materials and Methods for details). Eighty-seven EGFR interactions identified by a modified MYTH approach were rendered with NAViGaTOR 2.1.14 (http://ophid.utoronto.ca/navigator), where nodes in a graph correspond to proteins and edges represent physical protein-protein interactions. Node color corresponds to the GO terms annotating each protein in SwissProt version 51.5, and mapped to one of 11 categories as shown in the key. Square nodes signify membrane-associated and integral membrane proteins as defined by GO "Cellular Component" terms and SwissProt keywords. Edge color corresponds to source of interaction; blue edges represent MYTH interactions, and red edges correspond to interactions from I²D. Thicker edges signify multiple sources for a given interaction, whereas dashed edges are interactions supported only by one source: Dashed blue edges were previously unknown interactions identified by MYTH, and thick blue edges are MYTH interactions that were already present in I²D version 1.71. Dashed red edges have only one source of support in I²D, and thick red edges have two or more sources for the interactions. The XML file (Figure 1A_NAViGaTOR_XML) for visualization of the EGFR-interaction network with NAViGaTOR (40) is available online (http://www.cs.utoronto.ca/~juris/data/SciSig09). (**B**) Venn diagram showing the intersection of 403 EGFR interactions from the three main sources:

two published reports (5, 6), interactions from I²D version 1.71, and MYTH. (**C**) Interaction of selected putative binding partners. Cell lysates from serum-starved (control) or EGF-stimulated A431 cells were immunoprecipitated (IP) with an antibody that recognizes EGFR. Samples were immunoblotted and probed with antibodies to the indicated proteins. Probe with EGFR antibody shows equal efficiency of immunoprecipitation. IgG, immunoglobulin G.

denotes the minimal interaction domain between the two proteins (Fig. 2B). To confirm these observations, various FLAG-tagged HDAC6 deletion mutants were coexpressed with EGFR in HEK293T cells and were immunoprecipitated with FLAG antibody. All HDAC6 constructs coimmunoprecipitated EGFR, except the HDAC6 mutant consisting of residues 1 to 840 (fig. S4D). A similar approach was used to map the HDAC6 binding site on the EGFR. Deletion of the juxtamembrane region of EGFR-C-T (corre-

sponding to amino acids 645 to 672 of mature human EGFR) completely abolished the interaction with HDAC6, suggesting that the HDAC6 binding site on EGFR is at the juxtamembrane region (Fig. 2C).

To analyze if HDAC6 also interacted with other transmembrane receptors or integral membrane proteins, we performed the MYTH assay with cotransformed yeast with plasmids encoding HDAC6 and different receptors. We detected binding of HDAC6 to other ErbB family members, ErbB2,

Fig. 2. HDAC6 is a previously unknown EGFR interactor. (**A**) A bait-dependency MYTH assay shows the specificity of the HDAC6-EGFR interaction. THY.AP40 yeast expressing MFα-EGFR-C-T (left panel) or the unrelated human transferrin receptor (T-C-TFRC, right panel) was transformed with NubG-HDAC6. Yeast growth was assayed on selective media with or without X-gal as indicated. A known EGFR interactor [glyceraldehyde-3-phosphate dehydrogenase (GAPDH)] fused to NubG and Fur4-NubI were positive controls and a noninteracting protein GABAβ1A fused with NubG served as a negative control. (**B**) Amino acids 1010 to 1050 of HDAC6 bind to EGFR. THY.AP40 yeast was transformed with MFα-EGFR-Cub-TF and various HDAC6 prey constructs as indicated. Yeast growth was assessed on selective media with or without X-gal as indicated. A schematic representation of the two deacetylase domains (HDAC), the HDAC6 EGFR binding domain (HEBD), and the zinc finger Ub binding domain is shown. (**C**) The juxtamembrane region of the human EGFR interacts with HDAC6. The THY.AP40 yeast reporter strain was cotransformed with the indicated bait construct and control plasmids (Ost1-NubG and Ost1-NubI) and NubG-HDAC6. Interactions between HDAC6 and the EGFR truncations were assayed by spotting three independent transformants on selective and nonselective media. Yeast harboring the full-length MFα-EGFR-C-T and NubG-HDAC6 grew on SD-Trp-Leu-Ade-His and produced a strong blue signal on X-gal plates. This interaction between HDAC6 and EGFR was maintained among all EGFR truncations excluding MFα-EGFR644-C-T (bottom panel), suggesting that the HDAC6 binding site on EGFR involves the juxtamembrane region between mature EGFR residues 645 to 672. The schematic on the right illustrates the EGFR truncations with start residues corresponding to mature EGFR. EC, extracellular EGFR region; TM, transmembrane segment; JM, juxtamembrane region; TK, tyrosine kinase domain; RR, regulatory region; C-T, Cub-transcription factor (LexA-VP16); aa, amino acid.
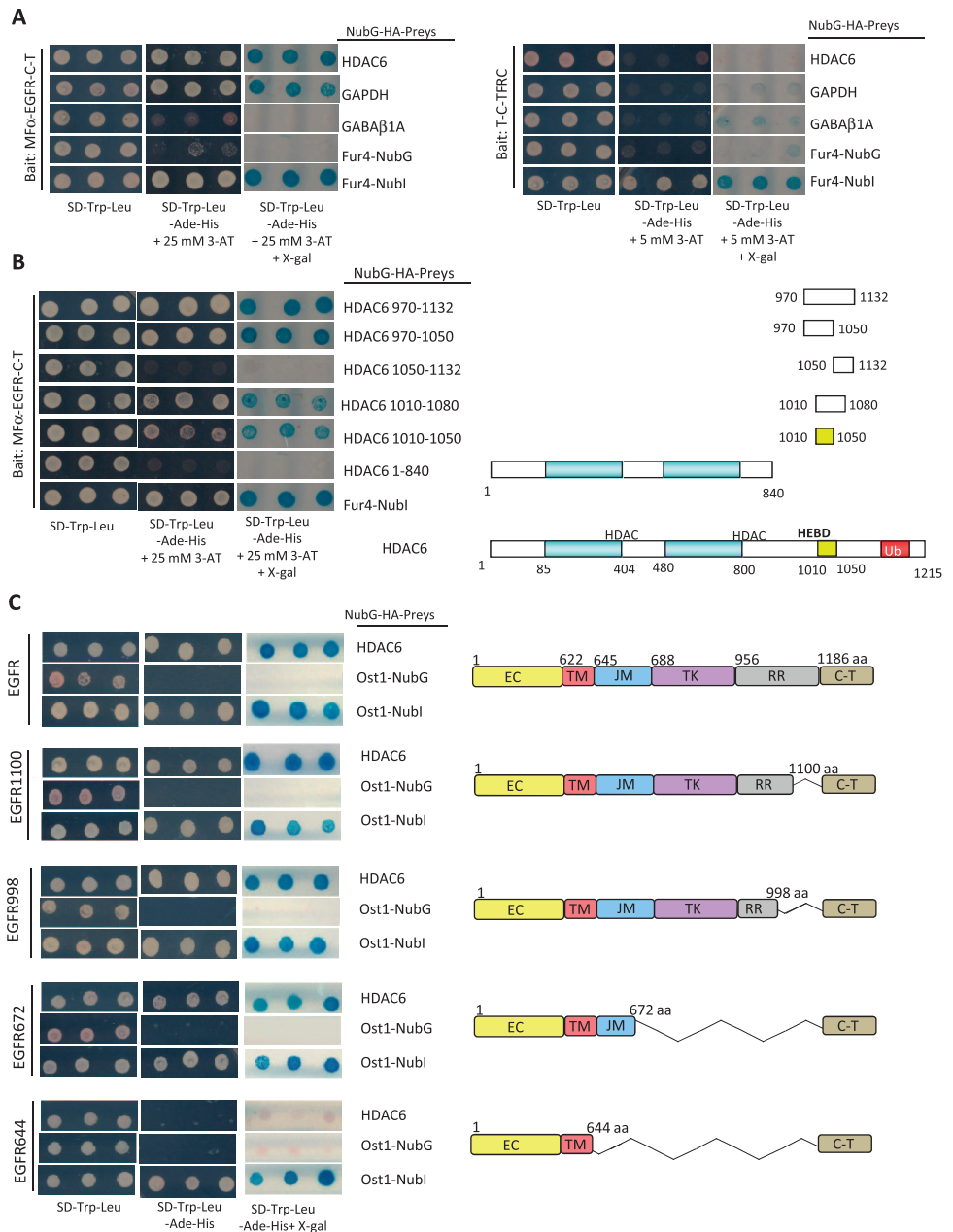
ErbB3, and ErbB4. However, we failed to detect an interaction with HDAC6 and other mammalian integral membrane proteins, such as the mouse transporters NHE3, NaPi-IIa, and MAP17 or the human ion channels SLC989 and SLC22A4, thus excluding the possibility that HDAC6 nonspecifically associates with other human integral membrane proteins that are also internalized through clathrin-coated pits (fig. S5).

HDAC6 regulates ligand-induced degradation of EGFR

We observed that overexpression of HDAC6 increased the abundance of EGFR in several cell lines (Fig. 3A and fig. S6). We monitored the abundance of endogenous EGFR after EGF stimulation in lung cancer–derived A549 cells that were transfected with FLAG-HDAC6 or a FLAG-HDAC6 mutant lacking deacetylase activity (HDAC6-H216A/H611A). HDAC6, but not HDAC6-H216A/H611A, stabilized EGFR in both non-stimulated and EGF-stimulated cells (Fig. 3A). We tested whether this stabilization was dependent on the ability of HDAC6 to bind to the receptor. Based on the experiments that identified the EGFR binding site on HDAC6 (Fig. 2B and fig. S4D), we created an HDAC6 deletion mutant lacking residues 882 to 1022 (HDAC6-ΔHEBD), which should not bind to the EGFR (Fig. 2, B and C). HDAC6-ΔHEBD had a much weaker sta-
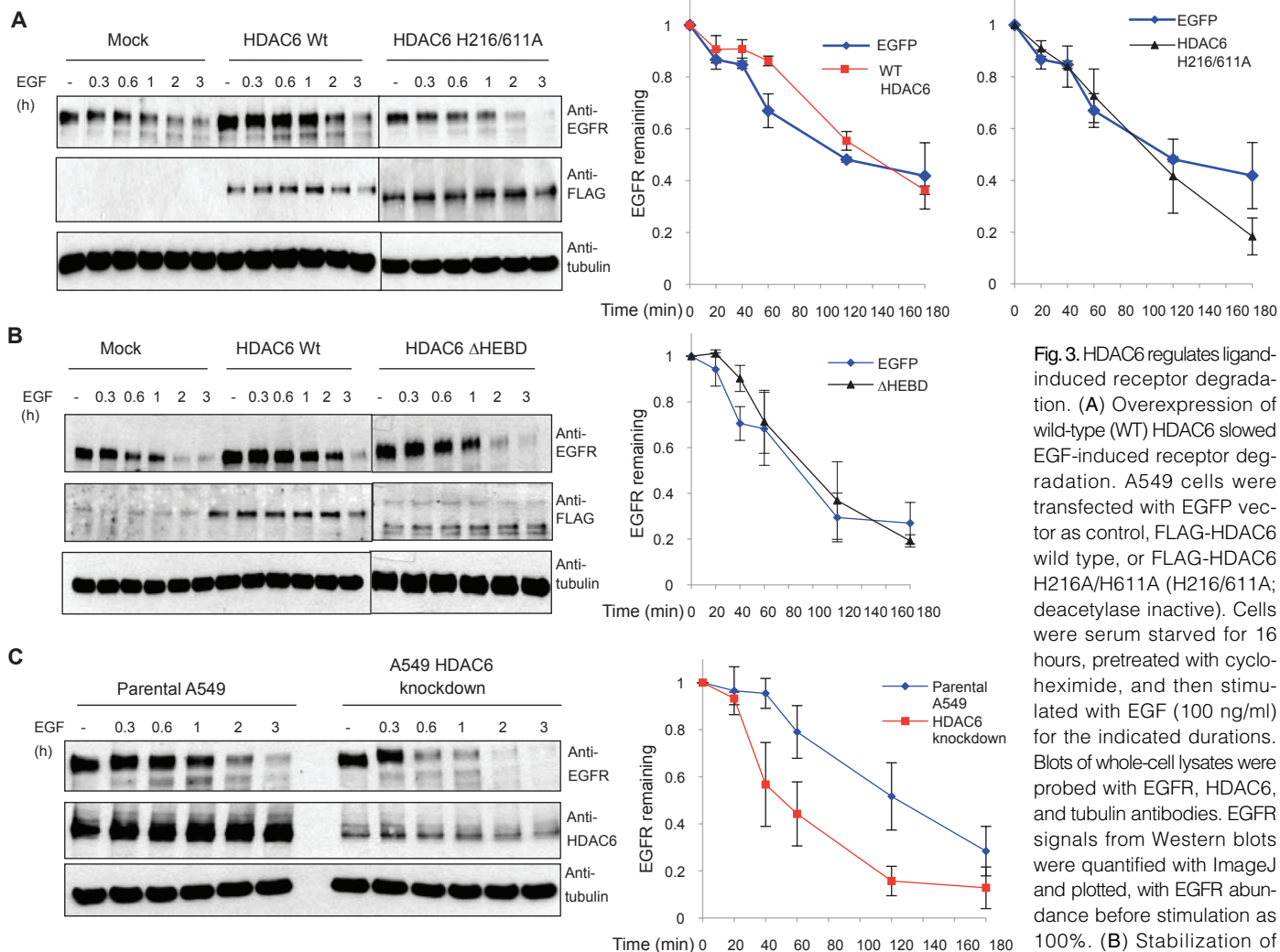
Fig. 3. HDAC6 regulates ligand-induced receptor degradation. (**A**) Overexpression of wild-type (WT) HDAC6 slowed EGF-induced receptor degradation. A549 cells were transfected with EGFP vector as control, FLAG-HDAC6 wild type, or FLAG-HDAC6 H216A/H611A (H216/611A; deacetylase inactive). Cells were serum starved for 16 hours, pretreated with cycloheximide, and then stimulated with EGF (100 ng/ml) for the indicated durations. Blots of whole-cell lysates were probed with EGFR, HDAC6, and tubulin antibodies. EGFR signals from Western blots were quantified with ImageJ and plotted, with EGFR abundance before stimulation as 100%. (**B**) Stabilization of EGFR by HDAC6 depends on the presence of the HDAC6 EGFR-binding domain (HEBD). A549 cells were transfected with an EGFP vector as control, FLAG-HDAC6 wild type, or FLAG-HDAC6 ΔHEBD. EGFR degradation was monitored and quantified as in (A). (**C**) HDAC6 knockdown accelerated degradation of EGFR after ligand stimulation. Control A549 and HDAC6 stable knockdown cells were serum starved for 16 hours and pretreated with cycloheximide and EGF (100 ng/ml) for the indicated durations. Cell lysates were run on SDS-PAGE and blots were probed with an EGFR antibody. Probing with antibodies that recognize HDAC or tubulin show the efficiency of knockdown and equal loading, respectively. EGFR signals from three experiments was quantified and plotted as in (A) and (B).

bilization effect on ligand-induced EGFR degradation compared to that of wild-type HDAC6 (Fig. 3B).

To further examine the effect of HDAC6 on the dynamics of EGFR degradation, we used A549 parental and A549 cells with short hairpin RNA (shRNA)–mediated knockdown of HDAC6. Cells were serum starved for 16 hours and de novo protein synthesis was inhibited by cycloheximide treatment. The cells were then stimulated with EGF for 20 to 180 min and lysates were probed to determine the abundance of EGFR. In control cells, receptor degradation initiated at ~1 hour and progressively continued to 3 hours, whereas in HDAC6 knockdown cells, degradation of EGFR started earlier (at 40 min) and was essentially complete within 2 hours (Fig. 3C). The knockdown of HDAC6 caused a much more dramatic effect on EGFR degradation than did the overexpression of HDAC6, which may be due to the high abundance of endogenous HDAC6 whereby

a gain-of-function experiment will have lower incremental effect than a loss-of-function approach.

HDAC6 modulates the dynamics of the motility of endosomes carrying EGFR

A primary mechanism of terminating EGFR activity is ligand-induced receptor internalization followed by endosomal trafficking and subsequent degradation in lysosomes (7). Using a receptor internalization assay with radioactive iodine (^{125}I)–labeled EGF, we did not see a significant difference in the rate of receptor internalization in Chinese hamster ovary (CHO) cells overexpressing wild-type or a deacetylase-deficient mutant of HDAC6 relative to that in control cells (Fig. 4A). However, HDAC6 might influence the trafficking and sorting of the receptor along the endocytic route. Indeed, HDAC6 partially colocalized with EGF-
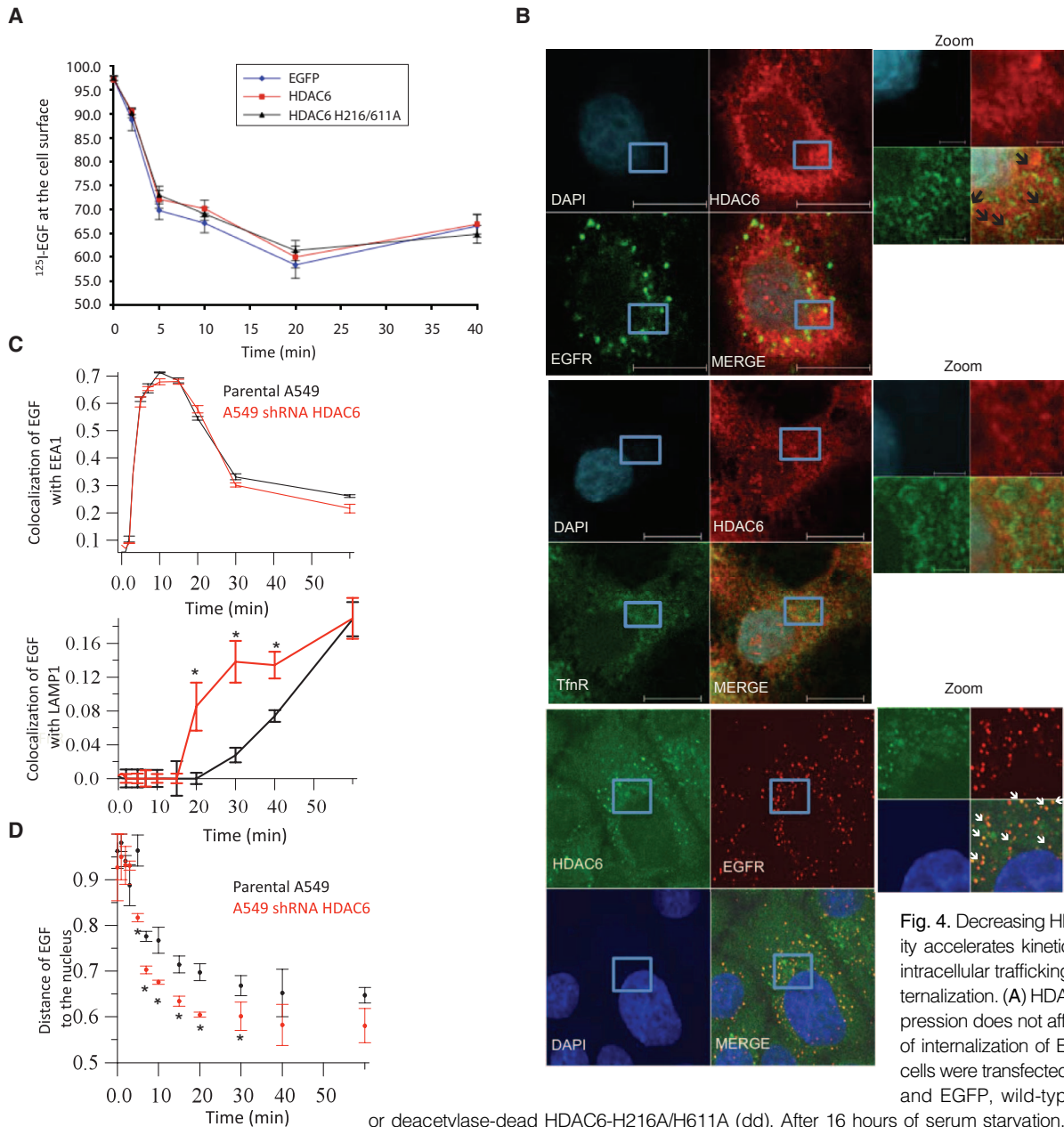
Fig. 4. Decreasing HDAC6 activity accelerates kinetics of EGFR intracellular trafficking but not internalization. (**A**) HDAC6 overexpression does not affect the rate of internalization of EGFR. CHO cells were transfected with EGFR and EGFP, wild-type HDAC6, or deacetylase-dead HDAC6-H216A/H611A (dd). After 16 hours of serum starvation, cells were stimulated with EGF (50 ng/ml) for the durations indicated. The amount of radioactive EGF-EGFR complex left at the cell surface was measured with ^{125}I-labeled EGF (1 ng/ml) normalized to the amount of EGFR at time point 0 (steady state) and plotted versus time of stimulation. (**B**) HDAC6 and EGFR colocalize in intracellular vesicles after EGF stimulation. Confocal microscopy using serum-starved HeLa cells exposed to EGF–Alexa 547 (green, top) or human holotransferrin–Alexa 547 for 60 min at 37°C (green, middle). HDAC6 was visualized by immunostaining (red). HeLa cells were transfected with Rab5 Q79L (bottom), allowed to endocytose EGF–Alexa 555 (red), and immunostained with HDAC6 antibody (green). Images in zoom show higher magnification (scale bar is 2 μm) of representative vesicular signals with arrows (top and bottom) indicating some of the vesicles staining positive for EGF and HDAC6. (**C**) EGF delivery to late endosomes is accelerated in HDAC6-knockdown cells. Serum-starved A549 cells were pulsed with EGF–Alexa 488, chased for the indicated times, and immunostained with EEA1 or LAMP1 antibodies. Endosomes were identified by MotionTracker, and parameters for localization, number, and size were computed. Graphs show the percentage of EGF colocalized with EEA1- or LAMP1-positive vesicles versus time in control (black) and knockdown cells (red). *$P < 0.05$, t test. (**D**) Internalized EGF approached the perinuclear area rapidly in HDAC6-knockdown cells. Data generated in EGF pulse-chase experiments were analyzed to quantify the distance of EGF-positive vesicles from the nucleus in units of nuclear size.

bound EGFR in vesicular structures upon ligand stimulation (Fig. 4B, upper panel, and fig. S6) but not with transferrin receptor that is predominantly in recycling vesicles (Fig. 4B, middle panel). To show that HDAC6 is localized on endosomes carrying EGF-bound EGFR, we induced the formation of enlarged early endosomes by transfection of the guanosine triphosphatase–deficient mutant Rab5 Q79L (19) and observed colocalization of HDAC6 with the EGFR complexes in the endosome (Fig. 4B, lower panel).

We performed a pulse-chase experiment using Alexa 488–labeled EGF as a ligand to further dissect the spatiotemporal influence of HDAC6 on the kinetics of EGFR trafficking in cells. Parental A549 cells or cells expressing shRNA against HDAC6 (Fig. 3C) were pulsed with Alexa 488–EGF for 30 s and chased for various periods of time. The EEA1 (early endosomal antigen 1) and LAMP1 (lysosome-associated membrane protein 1, a marker of late endosomes and lysosomes) were visualized by immunostaining, and four-channel laser confocal microscopy images were acquired from at least 10 fields with an average of 10 cells per field. After vesicles marked with Alexa 488–EGF, EEA1, or LAMP1 were identified, we quantified endosome number, size, intensity, colocalization between the different markers, and spatial distribution (20). Similar to the internalization assay with ^{125}I-labeled EGF, knockdown of HDAC6 did not affect entry of EGF into EEA1-positive early endosomes (Fig. 4C, upper graph). However, knockdown of HDAC6 accelerated the delivery of EGF into LAMP1-positive late endosomes and lysosomes, as visualized by increased colocalization of EGF with LAMP1 (Fig. 4C, lower panel). Furthermore, the distance between the EGF-containing endosomes and the nucleus decreased much faster, showing that the rate of travel toward the center of the cell was increased (Fig. 4D). These observations are consistent with the accelerated degradation of EGFR in HDAC6-knockdown cells (Fig. 3C). In addition, we observed increased integral vesicular intensity of EEA1-positive vesicles for EGF-bound EGFR in knockdown cells, demonstrating more content in these endosomes (fig. S8). Early endosomes progressively increase in size, concentrate cargo destined for degradation, and adopt a more central location in cells before conversion into late endosomes and before fusing with lysosomes (20). Thus, the increased colocalization of EGFR with LAMP1, decreased endosome-nucleus distance, and increased content of endosomes in cells in which HDAC was knocked down is consistent with a model of faster transport of EGFR-carrying endosomes toward the perinuclear area where receptor degradation occurs (7, 8).

EGFR activation induces tyrosine phosphorylation and inhibition of HDAC6 leading to increased acetylation of α-tubulin

Because the stabilization of EGFR requires HDAC6 deacetylase activity (Fig. 3A), we hypothesized that ligand-induced acetylation might regulate the kinetics of receptor trafficking. A systematic search for acetylated proteins in complex with EGFR and in the endocytic apparatus was performed primarily by immunoprecipitating EGFR from cells treated with the HDAC inhibitor trichostatin A (TSA) and subjecting the immunoprecipitates to mass spectrometric analysis to look for acetylated peptides. Additionally, individual endocytic proteins implicated in regulating EGFR endocytosis, including c-Cbl, CIN85, epsin, eps-15, and HRS were immunoprecipitated and immunoblotted with an acetyl lysine–specific antibody. Despite this search for potential substrates of HDAC6 in the endocytic apparatus, we failed to find any acetylated lysines that could be modulated by HDAC6 in a protein involved in postinternalization trafficking of the receptor. Because HSP90 is a substrate of HDAC6 and is involved in maturation of various signaling molecules (16), we tested whether HSP90 regulated ligand-induced EGFR degradation. Although HSP90 is implicated

in maturation of the ErbB family member ErbB2 and mutants of EGFR, wild-type EGFR is not influenced by HSP90 activity (21–23).

We used A549 cells that were serum starved and cycloheximide treated to inhibit new protein synthesis, then left untreated or treated with HSP90 inhibitor geldanamycin for 4 hours. After addition of EGF for different durations, we lysed the cells and measured the abundance of EGFR by Western blots (fig. S9). As shown, inhibition of HSP90 had no effect on the ligand-induced degradation of EGFR; thus, it is unlikely that the effect of HDAC6 on trafficking is mediated by changes in the acetylation status of HSP90.

In contrast, we detected, by mass spectrometric analyses, an increase in the acetylation of α-tubulin on lysine residue 40 (Lys^{40}) after EGF stimulation (Fig. 5A and fig. S10). The intensity of the peptide containing acetylated Lys^{40} (peptide 8 in Fig. 5A) was 2.3-fold higher in EGF-stimulated cells compared to the basal level of acetylation of α-tubulin in nonstimulated cells. The ratio of the EGF-stimulated versus nonstimulated intensities of nonmodified tubulin peptides (peptides 1 to 7; Fig. 5A) was ~1, indicating that equivalent amounts of total α-tubulin were analyzed.

Acetylation of Lys^{40} in α-tubulin enhances the interaction between microtubules and the motor proteins kinesin and dynein, thus accelerating the transport of cargo proteins in the secretory pathway (24, 25). To test whether acetylation of α-tubulin Lys^{40} similarly affects movement of early endosomes along microtubules, we used live-cell imaging by spinning disc microscopy (see Materials and Methods for detail and movie S1). mCherry-α-tubulin or a mCherry-α-tubulin-K40A was expressed in A431 cells stably transfected with low amount of GFP-Rab5 and the speed and number of processive movements of individual Rab5 endosomes were calculated. Either α-tubulin construct has previously been shown to incorporate into microtubules (25), and the α-tubulin-K40A has dominant-negative activity that reduces acetylation of microtubules (26). We found that cells expressing the α-tubulin-K40A mutant displayed a statistically significant reduction in speed (Fig. 5B) and processivity of Rab5 endosomes (Fig. 5C), compared to cells expressing wild-type α-tubulin. Thus, stimulation of EGFR increased acetylation of tubulin, and acetylation influenced the kinetics of microtubule-mediated endosomal trafficking, thereby suggesting a link between acetylation and EGFR trafficking.

We investigated potential molecular mechanisms involved in the increase of acetylation of tubulin. One possible explanation was that the activity of HDAC6 was decreased after EGFR activation. Because several members of the HDAC family are regulated by phosphorylation (27–29), we hypothesized that HDAC6 may also be influenced by phosphorylation. We performed a comprehensive mass spectrometric analysis of HDAC6 and identified two phosphorylated peptides, one containing Ser^{563}, Ser^{564}, and Ser^{568} and another containing Tyr^{570}. To determine which phosphorylation site was modulated by EGFR activation, HeLa cells were serum starved and subsequently stimulated for various time points with the EGF ligand. We immunoprecipitated HDAC6, using an HDAC6-specific antibody, and probed the blots with phosphoserine or phosphotyrosine antibodies. We saw a progressively increasing phosphotyrosine signal (Fig. 5D), suggesting HDAC6 Tyr^{570} is modulated by EGFR activation. Blotting the cell lysates for acetylation of α-tubulin on Lys^{40} revealed a corresponding gradual increase in acetylation, indicating phosphorylation might have an inhibitory role on the activity of HDAC6 (Fig. 5E). We assessed whether HDAC6 was a substrate for EGFR kinase activity with an in vitro kinase assay and found that purified recombinant HDAC6 was phosphorylated by EGFR in a concentration-dependent manner by purified glutathione S-transferase (GST)–EGFR kinase domain, only in the presence of adenosine triphosphate (ATP; Fig. 5F). To directly show that HDAC6 Tyr^{570} plays a crucial role by regulating its enzymatic activity,

Fig. 5. EGFR-induced phosphorylation of HDAC6 regulates its tubulin deacetylase activity. (**A**) Mass spectrometry revealed increased Lys[40] acetylation of tubulin after EGF stimulation. HeLa cells were serum starved for 16 hours and stimulated with EGF. Lysates were subjected to immunoprecipitation (IP) with a tubulin antibody and samples were prepared for and analyzed by mass spectrometry as described in Materials and Methods. Graph shows the ratio of peptide abundance from each sample with EGF stimulation compared with peptides from non-stimulated cells. The peptides analyzed: 1, DGQMPSDKTIGGGD; 2, DKTIGGG; 3, DKTIGGGD; 4, DKTIGGGDDSFNTFFSETGAG-KHVPRAVFV; 5, DLEPTVI; 6, DCAFMVDNEAIY; 7, DICRRNL; 8, DK*TIGGGD (peptide containing acetylated Lys[40]). Abbreviations for the amino acids are as follows: A, Ala; C, Cys; D, Asp; E, Glu; F, Phe; G, Gly; H, His; I, Ile; K, Lys; L, Leu; M, Met; N, Asn; P, Pro; Q, Gln; R, Arg; S, Ser; T, Thr; V, Val; and Y, Tyr. (**B**) GFP-Rab5 endosomes moved slowly in cells expressing the dominant-negative K40A-mutated tubulin. Fast live-cell imaging and individual endosome tracking was performed in A431-GFP-Rab5 cells overexpressing wild-type (WT) and K40A-mutant mCherry-tubulin.

The speed of GFP-positive early endosomes was computed and graphed. Student's *t* test for statistical significance was performed; **$P < 0.05$. (**C**) Efficient processive movement of endosomes depends on Lys[40] of tubulin. Live-cell imaging was performed as in Fig. 4D. Processive movement of Rab5 endosomes was computed and plotted. Student's *t* test for statistical significance was performed. *$P = 0.08$; **$P < 0.05$. (**D**) HDAC6 is phosphorylated on tyrosine residues upon EGFR activation. HeLa cells were serum starved, pretreated with sodium orthovanadate, and EGF stimulated for the indicated durations. After immunoprecipitation with HDAC6 antibodies and stringent washes, blots were probed with antibodies against phosphotyrosine or HDAC6. (**E**) Acetylation of α-tubulin Lys[40] increased gradually after EGFR activation. Total cell lysates from EGF-stimulated HeLa cells as in (B) were subjected to Western blotting and probed with antibodies against acetyl Lys[40] (K40) tubulin or tubulin. (**F**) HDAC6 is phosphorylated by the EGFR kinase domain. In vitro kinase assay was performed with purified recombinant HDAC6 (4 μM) and GST-EGFR kinase domain (KD) (2, 10, and 20 nM) with
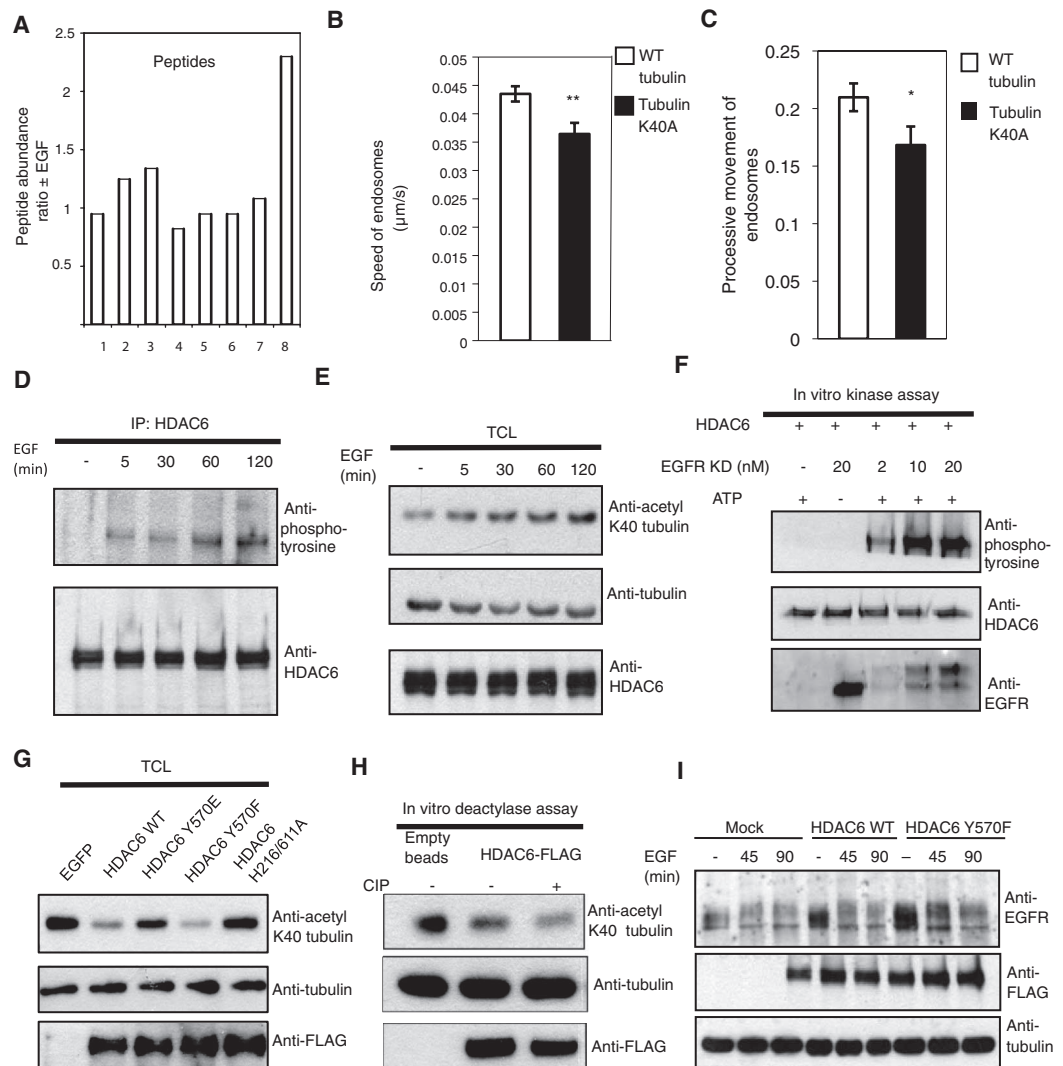
and without ATP. The reactions were stopped with SDS-PAGE loading buffer and loaded on gels. Blots were probed with phosphotyrosine, HDAC6, and EGFR antibodies. (**G**) Phosphorylation mimicking mutant of HDAC6 on Tyr[570] abolished its deacetylase activity. An EGFP vector, FLAG-HDAC6 wild type (WT), FLAG-HDAC6 Y570E (phopsphorylation mimicking), FLAG-HDAC6 Y570F (nonphosphorylatable), and FLAG-HDAC6 H216/611A (deacetylase inactive) plasmids were transfected in HEK293T cells. Cell lysates were probed with acetyl K40 tubulin, FLAG, and tubulin antibodies. (**H**) Dephosphorylation of HDAC6 enhanced its enzymatic activity. Purified assembled microtubules were incubated with empty beads (lane 1), immunopurified HDAC6 (lane 2), or HDAC6-treated with CIP (lane 3). Blots were probed for tubulin acetylated on Lys[40], total tubulin, and FLAG-HDAC6. (**I**) Stabilization of EGFR by HDAC6 Y570F. EGFP, HDAC6 WT, or HDAC6 Y570F were transfected into HeLa cells and EGFR degradation was monitored as described in Fig. 3. Experiments shown in (D) to (I) were performed three times.

we created a phosphomimicking mutant, Y570E, and a nonphosphorylatable mutant, Y570F. In an in vivo deacetylase assay with acetylation of α-tubulin on Lys[40] as readout, we showed that enzymatic activity of the

phosphomimicking mutant was abolished, whereas the nonphosphorylatable mutant maintained activity comparable to that of wild-type HDAC6 (Fig. 5G). We also performed an in vitro deacetylase assay in which over-

expressed HDAC6 immunopurified from HEK293T cells was incubated with purified brain-derived microtubules in the presence or absence of calf intestinal phosphatase (CIP). Dephosphorylated HDAC6 was more active than untreated HDAC6 (Fig. 5H). Because HDAC6 Y570F cannot be phosphorylated and inactivated by EGFR, we hypothesized that this mutant of HDAC6 should have a stronger stabilization effect on EGFR than does wild-type HDAC6. Comparison of mock-, wild-type HDAC6-, or HDAC6 Y570F–transfected cells revealed that cells expressing the HDAC6 Y570F mutant exhibited the greatest EGFR stabilization (Fig. 5I). Thus, phosphorylation of HDAC6 on Tyr[570] by EGFR inhibits the deacetylase activity of HDAC6, which results in the increased acetylation of α-tubulin after EGF stimulation.

DISCUSSION

We describe the identification of a set of proteins that interact with the full-length EGFR in its ligand-unoccupied state using a modified MYTH system. Our refinement of this technique facilitates the study of other mammalian single transmembrane proteins and their interactors. Use of this modified MYTH system with other receptor tyrosine kinases should result in a more complete map of protein-protein interactions linked to these receptors, the "receptor tyrosine kinase interactome."

One of the EGFR interactors identified with the modified MYTH system, the lysine deacetylase HDAC6, interacted with ligand-unoccupied EGFR in mammalian cells and regulated the kinetics of receptor trafficking in endosomes. HDAC6 also interacted with other ErbB family receptors (fig. S3). Others have reported that treatment of cells with histone deacetylase inhibitors or knockdown of HDAC6 with siRNA (small interfering RNA) leads to reduced steady-state abundance of vascular endothelial growth factor receptors (17), EGFR, and platelet-derived growth factor receptor α (30). Thus, it is possible that HDAC6 plays a broader role in stabilizing receptors, which may depend on its ability to interact with them. A major goal for the future is to identify other receptors that bind to HDAC6 and to define the biological significance of these interactions.

We identified α-tubulin as a critical HDAC6 substrate involved in the control of endosomal dynamics, although it is possible that there are other relevant substrates of HDAC6. In this context, the cellular acetylome consisting of a large number of cellular proteins was reported and a number of proteins, including those implicated in receptor trafficking and cytoskeletal dynamics such as c-Cbl and cofilin, were identified as acetylated on lysine residues (31). However, the acetylation of none of these endocytic proteins (except α-tubulin) was modulated by treatment of cells with HDAC inhibitors (31). This is in accordance with our work that identified only α-tubulin as the relevant target of HDAC6 in EGFR trafficking. However, it is possible that other groups of lysine deacetylases resistant to HDAC inhibitors could modulate the acetylation of the other proteins involved in endocytosis and thereby regulate their functions.

Mechanistically, the significant reduction in speed and processive motility observed in tubulin-K40A mutant could be explained by a decrease in acetylation of sites on the microtubules, which subsequently perturbed binding of motor proteins, such as dynein (24, 25). Quantitative EGF pulse-chase experiment showed that HDAC6 knockdown accelerated the delivery of EGF into late endosomes (Fig. 4C, right panel). Microtubules and the associated motor protein dynein promote fusion and fission events between endosomes, particularly during early to late endosome transport (32, 33). In this context, down-regulation of HDAC6 accelerated entry of EGF-bound EGFR into late endosomes, but not into early endosomes. Based on these observations, we believe that HDAC6

modulates the degradation of EGFR by deacetylating microtubules, thus decreasing the motility of cargo-carrying endosomes that move along microtubules toward the center of the cell. In this scenario, the effect of HDAC6 is likely a consequence of local accumulation of HDAC6 on the interface between the EGFR-loaded endosomes and microtubules. An additional layer of control operated through HDAC6 Tyr[570] phosphorylation by EGFR, which inhibited HDAC6 activity in vitro and in vivo. This represents a negative feedback loop whereby activation of EGFR is followed by inactivation of HDAC6 that is bound to the receptor on endosomes. In this process, HDAC6 is likely to play a fine-tuning role, which may explain the lack of gross developmental defects and obvious phenotypic changes in EGFR-dependent processes in HDAC6-knockout mice (34).

In summary, this study expands the role of reversible acetylation of proteins in the regulation of receptor trafficking. Given the interest in deacetylase inhibitors (HDACi) as anticancer therapeutics (35), it is tempting to speculate that a carefully planned combinatorial therapy that inhibits both EGFR receptor and HDAC6 could have a beneficial effect for treating selected types of cancers.

MATERIALS AND METHODS

Cell lines, EGF treatment, and transfection methods

HEK293T, CHO, HeLa, and A431 cell lines were purchased from the American Type Culture Collection and grown according to the supplier's instructions. A549 cells stably expressing shRNA for HDAC6 were established as previously described (36). A431 cells stably expressing GFP-Rab5 were previously described (20).

EGF was purchased from Peprotech. Cells were starved for 16 hours and then subjected to stimulation with EGF (100 ng/ml) for the indicated times. Alexa 555–EGF, Alexa 488–EGF, Alexa 647–EGF, human holotransferrin–Alexa 647 were from Invitrogen. For overexpression experiments, cells were transfected with Lipofectamine Reagent (Invitrogen), Effectene (Qiagen), or Fugene 6 HD (Roche) according to the manufacturer's instructions.

Constructs

Human EGFR excluding the first 24 amino acids was amplified by PCR and subcloned in MFα pAMBV empty vector (Dual Systems Biotech) by homologous recombination in yeast. Constructs for expressing wild-type and mutant HDAC6 are from the laboratory of T.-P. Yao of Duke University (36). mCherry-α-tubulin wild type and K40A were provided by F. Saudou, Institute Curie, Orsay, France, with approval by R. Tsien (University of California, San Diego) and described in (25). Plasmid encoding HA-FKBP38 was provided by the group of K. I. Nakayama of Kyushu University, Japan.

Antibodies and other reagents

Antibodies against HDAC6 (15) and against EGFR (37) were previously described. Another antibody against HDAC6 (H-300) and antibodies against ERK2 (C14) were purchased from Santa Cruz Biotechnology; antibodies against FLAG (M2), α-tubulin, or acetylated α-tubulin Lys[40], and polyclonal rabbit VP16 antibodies were obtained from Sigma. Cy2- and Cy5-labeled secondary antibodies were obtained from Jackson Immunoresearch. Antibody against HSP70 and TSA were from Cell Signaling Technologies. Other antibodies were antibodies against MAP3K12 or α-adaptin (Abcam), antibodies against GFP or LAMP1 (BD Pharmingen), and EEA1 antibodies (raised in the Zerial laboratory).

Membrane-based yeast two-hybrid screen

The yeast reporter strain THY.AP40 (*MATa trp1 leu2 his3 LYS2::lexA-HIS3 URA3::lexA-lacZ*) was transformed with the plasmid construct

MFα-EGFR-C-T bait by the lithium acetate protocol. Lack of self-activation of reporter genes was assessed, and then the correct integration of the protein into the plasma membrane was confirmed with Fur4-NubI/Fur4-NubG and Ost-NubI/Ost-NubG tests as previously described in detail (11, 13).

Human fetal brain complementary DNA (cDNA) library fused C-terminally to NubG (NubG-X orientation) were transformed into THY. AP40 yeast strain containing MFα-EGFR-C-T construct. About 3×10^7 TRP^+ LEU^+ transformants were selected on SD Leu⁻Trp⁻His⁻Ade⁻ medium containing 5 mM 3-aminotriazole (3-AT). Plasmids were isolated from 295 initial positive $HIS3^+/lacZ^+$ yeast colonies by the lyticase method and transformed into *Escherichia coli* DH5α with standard protocols. Selected library plasmids were retransformed into THY.AP40 expressing EGFR-C-T, TFRC-C-T, or empty bait vector as controls. The transformants were tested for the activation of the *lacZ* reporter by X-galactosidase (X-gal) filter lift-off assay after incubation for 3 hours at room temperature. Plasmids that activated the *HIS3* and *lacZ* reporters in combination with the EGFR-C-T bait were selected for sequencing and further studies.

Biochemical assays

For binding assays, HEK293T cells were transfected with the indicated constructs and lysed for 10 min on ice in lysis buffer [50 mM Hepes, 150 mM NaCl, 1 mM EDTA, 1 mM EGTA, 10% glycerol, 1% Triton X-100, 25 mM NaF, 10 μM $ZnCl_2$ (pH 7.5)] containing protease inhibitors (aprotinin, leupeptin, and phenylmethylsulfonyl fluoride). Cell lysates were collected, centrifuged for 15 min (13,000g) to remove the insoluble fraction, and incubated with the indicated antibodies for 2 to 4 hours at 4°C followed by 1 hour of incubation with protein A–Sepharose beads (Santa Cruz Biotechnology). The Sepharose matrix was then washed three times with lysis buffer. Bound proteins were analyzed by SDS–polyacrylamide gel electrophoresis (SDS-PAGE) and immunoblotting with the indicated antibodies. To detect acetylation, cells were treated with TSA for 2 hours, lysed, and immunoprecipitation was performed with the antibody against the protein of interest followed by immunoblotting with acetyl lysine–specific antibody. For ligand-induced EGFR degradation assays, A549 cells were serum starved, pretreated with cycloheximide (10 μg/ml) for 2 hours, and stimulated with EGF (100 ng/ml) for 20 to 180 min. After lysis, samples were run on SDS-PAGE and probed with EGFR antibody.

shRNA-mediated knockdown of HDAC6

Five different shRNA sequences targeting HDAC6 were introduced with lentiviruses (Sigma-Aldrich) into A549 cells. Of these, two resulted in substantial knockdown. The shRNA sequence used in the experiments is CCGGCATCC-CATCCTGAATATCCTTCTCGAAAGGATATTCAGGATGG-GATGTTTTT. Control cells were transduced with lentivirus encoding a sequence not found in human genome (CCGGCAACAAGATGAAGAGC-ACCAACTCGAGTTGGTGCTCTTCATCTTGTTGTTTTT).

Tubulin deacetylase assay

HEK293T cells expressing FLAG-tagged HDAC6 were lysed in the above-mentioned lysis buffer and immunoprecipitation was performed with the M2-FLAG antibody followed by stringent washing. CIP was added in Pipes buffer to the beads and washed away after incubation for 1 hour at 37°C. Taxol-stabilized, purified brain-derived microtubules (50 μg) were then added to the beads in 10 mM tris-HCl (pH 8), 10 mM NaCl buffer and incubated for 2 hours at 37°C. Subsequently, the reaction mixtures were spun down, loaded on SDS-PAGE, and probed with acetylated α-tubulin Lys⁴⁰ antibody and reprobed with an antibody that recognizes tubulin.

Immunofluorescence microscopy

Alexa 488–EGF pulse-chase experiments were performed by starving A549 cells (control and HDAC6 knockdown) for 16 hours, followed by a 30-s pulse of Alexa 488–EGF (100 ng/ml) and chase for 0, 1, 2, 3, 5, 7, 10, 20, 30, and 60 min. Holotransferrin–Alexa 6 47 was used at 25 μg/ml. Cells were fixed with paraformaldehyde, permeabilized, and immunostained for HDAC6. Images with Z-stacks were acquired with the Zeiss 510 UV confocal microscope at the same laser output for all images. Vesicles were identified by the MotionTracker program and the various parameters were examined.

Mass spectrometry

Tubulin-containing gel bands were cut out from the SDS-PAGE and subjected to reduction and alkylation with 10 mM dithiothreitol and 55 mM iodoacetamide (Sigma-Aldrich), respectively. Bands were washed with 50 mM ammonium bicarbonate and in-gel digested with endoproteinase Asp-N (Roche) for 16 hours at 37°C. Samples were analyzed by online C18 reversed-phase nanoscale liquid chromatography–tandem mass spectrometry (MS/MS) essentially as described (38). Briefly, analyses were performed on an Agilent 1200 nanoflow system (Agilent Technologies) connected to an LTQ-Oribitrap XL (ThermoFisher) equipped with a nanoelectrospray ion source (Proxeon Biosystems). The MS/MS spectra were centroided and searched with Mascot (MatrixScience) against the human International Protein Index (IPI) protein database (http://www.ebi.ac.uk/IPI/). Search parameters included mass tolerance of 6 parts per million for peptides and 0.6 dalton for fragments, Carbamidomethyl (C) as fixed modification and Oxidation (M) and Acetyl (K) as variable modifications. The intensities of the acetylated Lys⁴⁰-containing peptide derived from the nonstimulated and EGF-stimulated cells were used to calculate a ratio reflecting the relative levels of Lys⁴⁰ acetylation between the two samples. The intensity ratios of seven distinct nonmodified tubulin peptides were used for normalization.

EGFR internalization assay with ¹²⁵I-labeled EGF

EGFR trafficking dynamics was analyzed as previously described (39). In brief, CHO cells were transiently transfected with EGFR and HDAC6 constructs, as well as a GFP vector as a negative control. Two days after transfection, receptor trafficking was induced by EGF ligand stimulation at 37°C for the indicated times and then the cells were transferred to ice. The amount of EGFR molecules present at the cell surface was determined by removal of receptor-bound EGF by mild acidic treatment and incubation with ¹²⁵I-labeled EGF (1 ng/ml) for 1.5 hours. Cells were washed vigorously and lysed, and samples were analyzed with a gamma counter (1470 Wizard, Perkin Elmer). The percentage of surface receptor was calculated by comparison to samples challenged with EGF on ice only.

Live-cell imaging

A431 cells stably expressing GFP-Rab5 were grown in glass-bottomed dishes and were transfected with mCherry-tubulin wild type or the dominant-negative mCherry-tubulin K40 (20). Twenty-four hours later, dishes containing cells were imaged while maintaining the temperature at 37°C. Imaging was done with a custom-assembled microscope at the Max-Planck-Institute for Cell Biology and Genetics in Dresden, Germany. The microscope uses spinning-disc technology for laser beam focusing and connected with a high-speed camera for image acquisition. Cells were imaged for 5 min (four images per Z-stack, two stacks per second). Z stacks were collapsed by maximum projection. Fluorescence tracing with intensity were quantified for individual GFP-Rab5 endosomes by MotionTrack software. Statistical analysis was done to arrive at the cumulative average speed and processive movement of vesicles essentially as in Rink *et al.* (20).

Bioinformatic analysis

We mapped all proteins from MYTH screen into SwissProt identifiers and integrated the results with protein-protein interactions (PPIs) in Interologous Interaction Database (I²D) version 1.71 (http://ophid.utoronto.ca/i2d). Mapping was done with the following source databases: the IPI version 3.36 (http://www.ebi.ac.uk/IPI/), SwissProt version 51.5, Unigene Hs.208, and Entrez Gene 2007-02-08. Interactions in I²D integrate from human curated sources, high-throughput mammalian experiments, and predicted PPIs with orthologs from model organism protein interaction data sets, as previously described (*41*, *42*). Computational evidence provided support to the experimentally derived PPIs with the following procedure, performed essentially as previously described (*42*). First, we constructed a domain-domain co-occurrence matrix by extracting all InterPro domains from UniProt version 9.5 and enumerating the number of times each domain pair occurs between proteins known to interact or those that have not been experimentally shown to interact. Domain pairs that occurred more frequently between interacting proteins were identified using the hypergeometric distribution with a Bonferroni-corrected alpha level of 0.05. The resulting domain-domain co-occurrence set included 10,391 domain pairs significantly enriched in known human PPIs. Second, gene coexpression was calculated with the Pearson correlation between genes encoding the interacting proteins from the GeneAtlas expression compendium (*43*), which profiles gene expression on 79 human tissues. Finally, functional similarity was computed for all PPIs using GO annotations (*44*). Briefly, GO terms were retrieved from the UniProt database (version 9.5) for each of the interacting proteins and the semantic similarity (*45*) was computed.

To establish a threshold above which the aforementioned evidence was statistically significant, 65,535 random protein pairs were selected from the set of proteins that comprise the known human interactome. Each evidence type was computed for every random protein pair, and the threshold for statistical significance was derived from the 95% confidence interval of the resulting distributions.

The protein-protein interaction network was visualized with NAViGaTOR version 2.1.14 (http://ophid.utoronto.ca/navigator) (*40*).

SUPPLEMENTARY MATERIALS

www.sciencesignaling.org/cgi/content/full/2/102/ra84/DC1
Fig. S1. Generation and characterization of EGFR bait construct.
Fig. S2. Integrating EGFR-interacting proteins from multiple data sets.
Fig. S3. Validation of EGFR-interacting proteins identified in the MYTH screen.
Fig. S4. HDAC6 interacts with EGFR.
Fig. S5. HDAC6 interacts with other ErbB family members, but not with mammalian integral membrane transporters and ion channels.
Fig. S6. HDAC6 overexpression increases the abundance of EGFR.
Fig. S7. HDAC6 and EGFR partially colocalize at the plasma membrane, and in a fraction of intracellular vesicles following EGF stimulation.
Fig. S8. Downregulation of HDAC6 changes characteristics of endosomes.
Fig. S9. HSP90 inhibition has no discernible effect on ligand-induced degradation of EGFR.
Fig. S10. Identification of tubulin Lys⁴⁰ acetylation by mass spectrometry.
Tables S1 to S7. Annotation of EGFR-interacting proteins identified in MYTH and comparison to prior studies.
Movie S1. Live cell imaging of A431 cells stably expressing GFP-Rab5.
References
NAViGaTOR file for Figure 1A.

REFERENCES AND NOTES

1. A. Ullrich, J. Schlessinger, Signal transduction by receptors with tyrosine kinase activity. *Cell* **61**, 203–212 (1990).
2. Y. Yarden, M. X. Sliwkowski, Untangling the ErbB signalling network. *Nat. Rev. Mol. Cell Biol.* **2**, 127–137 (2001).
3. D. Hoeller, S. Volarevic, I. Dikic, Compartmentalization of growth factor receptor signalling. *Cur. Opin. Cell Biol.* **17**, 107–111 (2005).
4. T. Pawson, Specificity in signal transduction: From phosphotyrosine-SH2 domain interactions to complex cellular systems. *Cell* **116**, 191–203 (2004).
5. B. Blagoev, I. Kratchmarova, S. E. Ong, M. Nielsen, L. J. Foster, M. Mann, A proteomics strategy to elucidate functional protein-protein interactions applied to EGF signaling. *Nat. Biotechnol.* **21**, 315–318 (2003).
6. R. B. Jones, A. Gordus, J. A. Krall, G. MacBeath, A quantitative protein interaction network for the ErbB receptors using protein microarrays. *Nature* **439**, 168–174 (2006).
7. C. Le Roy, J. L. Wrana, Clathrin- and non-clathrin-mediated endocytic regulation of cell signalling. *Nat. Rev. Mol. Cell Biol.* **6**, 112–126 (2005).
8. D. J. Katzmann, G. Odorizzi, S. D. Emr, Receptor downregulation and multivesicular-body sorting. *Nat. Rev. Mol. Cell Biol.* **3**, 893–905 (2002).
9. K. Haglund, P. P. Di Fiore, I. Dikic, Distinct monoubiquitin signals in receptor endocytosis. *Trends Biochem. Sci.* **28**, 598–603 (2003).
10. Z. Galcheva-Gargova, K. N. Konstantinov, I. H. Wu, F. G. Klier, T. Barrett, R. J. Davis, Binding of zinc finger protein ZPR1 to the epidermal growth factor receptor. *Science* **272**, 1797–1802 (1996).
11. K. Iyer, L. Burkle, D. Auerbach, S. Thaminy, M. Dinkel, K. Engels, I. Stagljar, Utilizing the split-ubiquitin membrane yeast two-hybrid system to identify protein-protein interactions of integral membrane proteins. *Sci. STKE* **2005**, pl3 (2005).
12. I. Stagljar, C. Korostensky, N. Johnsson, S. te Heesen, A genetic system based on split-ubiquitin for the analysis of interactions between membrane proteins in vivo. *Proc. Natl. Acad. Sci. U.S.A.* **95**, 5187–5192 (1998).
13. C. M. Paumi, J. Menendez, A. Arnoldo, K. Engels, K. R. Iyer, S. Thaminy, O. Georgiev, Y. Barral, S. Michaelis, I. Stagljar, Mapping protein-protein interactions for the yeast ABC transporter Ycf1p by integrated split-ubiquitin membrane yeast two-hybrid analysis. *Mol. Cell* **26**, 15–25 (2007).
14. A. J. de Ruijter, A. H. van Gennip, H. N. Caron, S. Kemp, A. B. van Kuilenburg, Histone deacetylases (HDACs): Characterization of the classical HDAC family. *Biochem. J.* **370**, 737–749 (2003).
15. C. Hubbert, A. Guardiola, R. Shao, Y. Kawaguchi, A. Ito, M. Nixon, M. Yoshida, X. F. Wang, T. P. Yao, HDAC6 is a microtubule-associated deacetylase. *Nature* **417**, 455–458 (2002).
16. J. J. Kovacs, P. J. Murphy, S. Gaillard, X. Zhao, J. T. Wu, C. V. Nicchitta, M. Yoshida, D. O. Toft, W. B. Pratt, T. P. Yao, HDAC6 regulates Hsp90 acetylation and chaperone-dependent activation of glucocorticoid receptor. *Mol. Cell* **18**, 601–607 (2005).
17. J. H. Park, S. H. Kim, M. C. Choi, J. Lee, D. Y. Oh, S. A. Im, Y. J. Bang, T. Y. Kim, Class II histone deacetylases play pivotal roles in heat shock protein 90-mediated proteasomal degradation of vascular endothelial growth factor receptors. *Biochem. Biophys. Res. Commun.* **368**, 318–322 (2008).
18. A. Valenzuela-Fernández, S. Alvarez, M. Gordon-Alonso, M. Barrero, A. Ursa, J. R. Cabrero, G. Fernández, S. Naranjo-Suárez, M. Yañez-Mo, J. M. Serrador, M. A. Muñoz-Fernandez, F. Sánchez-Madrid, Histone deacetylase 6 regulates human immunodeficiency virus type 1 infection. *Mol. Biol. Cell* **16**, 5445–5454 (2005).
19. H. Stenmark, R. G. Parton, O. Steele-Mortimer, A. Lütcke, J. Gruenberg, M. Zerial, Inhibition of rab5 GTPase activity stimulates membrane fusion in endocytosis. *EMBO J.* **13**, 1287–1296 (1994).
20. J. Rink, E. Ghigo, Y. Kalaidzidis, M. Zerial, Rab conversion as a mechanism of progression from early to late endosomes. *Cell* **122**, 735–749 (2005).
21. W. Xu, E. Mimnaugh, M. F. Rosser, C. Nicchitta, M. Marcu, Y. Yarden, L. Neckers, Sensitivity of mature Erbb2 to geldanamycin is conferred by its kinase domain and is mediated by the chaperone protein Hsp90. *J. Biol. Chem.* **276**, 3702–3708 (2001).
22. A. Sawai, S. Chandarlapaty, H. Greulich, M. Gonen, Q. Ye, C. L. Arteaga, W. Sellers, N. Rosen, D. B. Solit, Inhibition of Hsp90 down-regulates mutant epidermal growth factor receptor (EGFR) expression and sensitizes EGFR mutant tumors to paclitaxel. *Cancer Res.* **68**, 589–596 (2008).
23. T. Shimamura, A. M. Lowell, J. A. Engelman, G. I. Shapiro, Epidermal growth factor receptors harboring kinase domain mutations associate with the heat shock protein 90 chaperone and are destabilized following exposure to geldanamycins. *Cancer Res.* **65**, 6401–6408 (2005).
24. N. A. Reed, D. Cai, T. L. Blasius, G. T. Jih, E. Meyhofer, J. Gaertig, K. J. Verhey, Microtubule acetylation promotes kinesin-1 binding and transport. *Curr. Biol.* **16**, 2166–2172 (2006).
25. J. P. Dompierre, J. D. Godin, B. C. Charrin, F. P. Cordelières, S. J. King, S. Humbert, F. Saudou, Histone deacetylase 6 inhibition compensates for the transport deficit in Huntington's disease by increasing tubulin acetylation. *J. Neurosci.* **27**, 3571–3583 (2007).
26. C. Creppe, L. Malinouskaya, M. L. Volvert, M. Gillard, P. Close, O. Malaise, S. Laguesse, I. Cornez, S. Rahmouni, S. Ormenese, S. Belachew, B. Malgrange, J. P. Chapelle, U. Siebenlist, G. Moonen, A. Chariot, L. Nguyen, Elongator controls the migration and differentiation of cortical neurons through acetylation of α-tubulin. *Cell* **136**, 551–564 (2009).
27. M. K. Pflum, J. K. Tong, W. S. Lane, S. L. Schreiber, Histone deacetylase 1 phosphorylation promotes enzymatic activity and complex formation. *J. Biol. Chem.* **276**, 47733–47741 (2001).

28. E. N. Pugacheva, S. A. Jablonski, T. R. Hartman, E. P. Henske, E. A. Golemis, HEF1-dependent Aurora A activation induces disassembly of the primary cilium. *Cell* **129**, 1351–1363 (2007).

29. R. Berdeaux, N. Goebel, L. Banaszynski, H. Takemori, T. Wandless, G. D. Shelton, M. Montminy, SIK1 is a class II HDAC kinase that promotes survival of skeletal myocytes. *Nat. Med.* **13**, 597–603 (2007).

30. K. Kamemura, A. Ito, T. Shimazu, A. Matsuyama, S. Maeda, T. P. Yao, S. Horinouchi, S. Khochbin, M. Yoshida, Effects of downregulated HDAC6 expression on the proliferation of lung cancer cells. *Biochem. Biophys. Res. Commun.* **374**, 84–89 (2008).

31. C. Choudhary, C. Kumar, F. Gnad, M. L. Nielsen, M. Rehman, T. C. Walther, J. V. Olsen, M. Mann, Lysine acetylation targets protein complexes and co-regulates major cellular functions. *Science* **325**, 834–840 (2009).

32. M. Bomsel, R. Parton, S. A. Kuznetsov, T. A. Schroer, J. Gruenberg, Microtubule- and motor-dependent fusion in vitro between apical and basolateral endocytic vesicles from MDCK cells. *Cell* **62**, 719–731 (1990).

33. F. Aniento, N. Emans, G. Griffiths, J. Gruenberg, Cytoplasmic dynein-dependent vesicular transport from early to late endosomes. *J. Cell Biol.* **123**, 1373–1387 (1993).

34. Y. Zhang, S. Kwon, T. Yamaguchi, F. Cubizolles, S. Rousseaux, M. Kneissel, C. Cao, N. Li, H. L. Cheng, K. Chua, D. Lombard, A. Mizeracki, G. Matthias, F. W. Alt, S. Khochbin, P. Matthias, Mice lacking histone deacetylase 6 have hyperacetylated tubulin but are viable and develop normally. *Mol. Cell. Biol.* **28**, 1688–1701 (2008).

35. S. Minucci, P. G. Pelicci, Histone deacetylase inhibitors and the promise of epigenetic (and more) treatments for cancer. *Nat. Rev. Cancer* **6**, 38–51 (2006).

36. Y. Kawaguchi, J. J. Kovacs, A. McLaurin, J. M. Vance, A. Ito, T. P. Yao, The deacetylase HDAC6 regulates aggresome formation and cell viability in response to misfolded protein stress. *Cell* **115**, 727–738 (2003).

37. R. M. Kris, I. Lax, W. Gullick, M. D. Waterfield, A. Ullrich, M. Fridkin, J. Schlessinger, Antibodies against a synthetic peptide as a probe for the kinase activity of the avian EGF receptor and v-erbB protein. *Cell* **40**, 619–625 (1985).

38. J. Dengjel, V. Akimov, J. V. Olsen, J. Bunkenborg, M. Mann, B. Blagoev, J. S. Andersen, Quantitative proteomic assessment of very early cellular signaling events. *Nat. Biotechnol.* **25**, 566–568 (2007).

39. M. H. Schmidt, I. Dikic, Assays to monitor degradation of the EGF receptor. *Methods Mol. Biol.* **327**, 131–138 (2006).

40. K. R. Brown, D. Otasek, M. Ali, M. J. McGuffin, W. Xie, B. Devani, I. L. van Toch, I. Jurisica, NAViGaTOR: Network Analysis, Visualization and Graphing Toronto. *Bioinformatics* **25**, 3327–3329 (2009).

41. K. R. Brown, I. Jurisica, Unequal evolutionary conservation of human protein interactions in interologous networks. *Genome Biol.* **8**, R95 (2007).

42. K. R. Brown, I. Jurisica, Online predicted human interaction database. *Bioinformatics* **21**, 2076–2082 (2005).

43. A. I. Su, T. Wiltshire, S. Batalov, H. Lapp, K. A. Ching, D. Block, J. Zhang, R. Soden, M. Hayakawa, G. Kreiman, M. P. Cooke, J. R. Walker, J. B. Hogenesch, A gene atlas of the mouse and human protein-encoding transcriptomes. *Proc. Natl. Acad. Sci. U.S.A.* **101**, 6062–6067 (2004).

44. M. Ashburner, C. A. Ball, J. A. Blake, D. Botstein, H. Butler, J. M. Cherry, A. P. Davis, K. Dolinski, S. S. Dwight, J. T. Eppig, M. A. Harris, D. P. Hill, L. Issel-Tarver, A. Kasarskis, S. Lewis, J. C. Matese, J. E. Richardson, M. Ringwald, G. M. Rubin, G. Sherlock, Gene ontology: Tool for the unification of biology. The Gene Ontology Consortium. *Nat. Genet.* **25**, 25–29 (2000).

45. P. W. Lord, R. D. Stevens, A. Brass, C. A. Goble, Semantic similarity measures as tools for exploring the gene ontology. *Pac. Symp. Biocomput.* 601–612 (2003).